

TRACKING THE STELLAR LONGITUDES OF STARSPOTS IN SHORT-PERIOD *KEPLER* BINARIES

BHASKARAN BALAJI¹, BRYCE CROLL^{2,3}, A. LEVINE², AND S. RAPPAPORT¹

Draft version September 9, 2021

ABSTRACT

We report on a new method for tracking the phases of the orbital modulations in very short-period, near-contact, and contact binary systems in order to follow starspots. We apply this technique to *Kepler* light curves for 414 binary systems that were identified as having anticorrelated $O - C$ curves for the midtimes of the primary and secondary eclipses, or in the case of non-eclipsing systems, their light-curve minima. This phase tracking approach extracts more information about starspot and binary system behavior than may be easily obtained from the $O - C$ curves. We confirm the hypothesis of Tran et al. (2013) that we can successfully follow the rotational motions of spots on the surfaces of the stars in these binaries. In $\sim 34\%$ of the systems, the spot rotation is retrograde as viewed in the frame rotating with the orbital motion, while $\sim 13\%$ show significant prograde spot rotation. The remaining systems show either little spot rotation or erratic behavior, or sometimes include intervals of both types of behavior. We discuss the possibility that the relative motions of spots are related to differential rotation of the stars. It is clear from this study that the motions of the starspots in at least 50% of these short-period binaries are not exactly synchronized with the orbits.

Subject headings: stars: binaries: close—stars: binaries: general—stars: rotation—stars: spots

1. INTRODUCTION

Among the many targets of the *Kepler* mission are some 700 short-period binary stellar systems (with orbital periods $\lesssim 2$ days), many of them contact binaries. These systems have orbital periods that are typically less than 0.5 days, and they are exemplary candidates for timing analyses of behavior related to eclipses or light-curve minima (in non-eclipsing systems). One such analysis involves the use of $O - C$ (“observed minus expected”) curves, i.e., the times of the eclipses or light-curve minima relative to those of a temporal reference system having a precisely constant period. Tran et al. (2013) investigated the particular phenomenon where the $O - C$ times for the primary and secondary minima oscillate in an anticorrelated manner, found some 390 binary systems displaying anti-correlated $O - C$ curves, and reported in detail on 32 of them. Tran et al. (2013) concluded that a model including starspots on one of the two stars is able to explain the anticorrelated $O - C$ curves. Their model implies or requires that the spots move slowly around their host stars in the reference frame rotating with the binary.

In the Tran et al. (2013) model, a spot on one of the stars produces a nearly sinusoidal variation of the apparent intensity as the binary system orbits. The frequency of the sinusoid must be very close to that of the stellar rotation with respect to inertial space. If the star with the spot nearly corotates with the binary, then the frequency of the variation will be close to the orbital frequency, ω . Since the light curves of many very short period binaries are dominated by a sinusoidal variation

at the frequency 2ω , the spot has the effect of slightly shifting the time of one light-curve minimum in a given direction, while shifting the time of the other light-curve minimum in the *opposite* sense. Hence, the spots can induce anticorrelated behavior in the $O - C$ curves. In this scenario, variations in the $O - C$ curves are caused by motion of the starspots in longitude in the rotating frame of the binary. An additional requirement Tran et al. (2013) presented was that the spots be visible at all times, i.e., not eclipsed by the companion star nor occulted by their host star. As far as we are aware, there are no viable alternative models to explain the anticorrelated $O - C$ behavior.

Despite showing that the starspot model could explain the anticorrelated $O - C$ behavior, Tran et al. (2013) did not attempt to actually track the sinusoidal variations of the inferred starspots. In this work, we seek to support the model by explicitly tracking these variations and the inferred stellar longitudes of the spots or groups of spots for the same 414 sources that showed anticorrelated $O - C$ curves, over the duration of the *Kepler* mission (~ 4 years; Borucki et al. 2010; Caldwell et al. 2010; Batalha et al. 2013). The orbital period distribution of the 414 binaries considered in this work is shown in Fig. 1.

Section 2 outlines the data used in this work and the preparation thereof. Sect. 3 presents the underlying model and demonstrates its effectiveness. Detailed analysis of a dozen systems, all exhibiting clear starspot motion is also presented. In Sect. 4, we compare our analysis with the previously generated, but updated, $O - C$ curves with the understanding that the two methods should, if they are indeed tracking the same phenomenon, provide similar information. In Sect. 5, we summarize our findings, and in Sect. 6, we demonstrate that the results may be used to search for third bodies among the *Kepler* short-period binary systems.

¹ M.I.T. Department of Physics and Kavli Institute for Astrophysics and Space Research, 70 Vassar St., Cambridge, MA, 02139; bbalaji@mit.edu; sar@mit.edu

² 37-575 M.I.T. Kavli Institute for Astrophysics and Space Research, 70 Vassar St., Cambridge, MA, 02139; croll@space.mit.edu; aml@space.mit.edu

³ 5525 Olund Road, Abbotsford, B.C. Canada

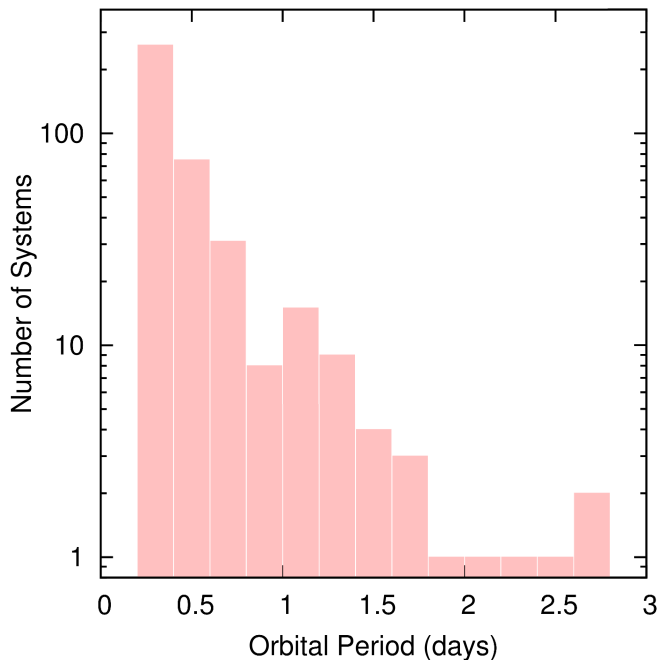


Figure 1. The orbital period distribution of 412 of the 414 *Kepler* binaries considered in this study. To improve the resolution of the plot two systems with periods longer than 3 days have been excluded. Please note the logarithmic scaling on the y-axis.

2. KEPLER DATA

The present study is based on *Kepler* long-cadence (LC) lightcurves, sets of sequential measurements of the flux obtained from 29.4-minute integrations. We retrieved the LC lightcurve files for Quarters 1 through 17 for all of the ~ 2600 candidates in the latest *Kepler* eclipsing binary catalog (Slawson et al. 2011; Matijevic et al. 2012) that were available at the Multimission Archive at STScI (MAST). We used the lightcurves made with the PDC-MAP algorithm (Stumpe et al. 2012; Smith et al. 2012), which is intended to remove instrumental signatures from the flux time series while retaining the bulk of the astrophysical variations of each target. For each quarter, the flux series was normalized to its median value. Then, for each target, the results from all available quarters were stitched together in a single flux data file.

We did not filter the data to remove long-term trends in the flux since the signal in the binary systems of interest is due to the relatively high-frequency binary orbital modulation and to the nearly corotating starspots. These are the two components that are analyzed in this work.

3. OVERVIEW OF THE MODEL

3.1. The Orbital Terms

The lightcurve of a very short period binary is often dominated by a sinusoid with a frequency twice that of the orbit, due to the very strong ellipsoidal light variations of the two stars that fill, or nearly fill, their Roche lobes. To the extent that the two stars have different effective temperatures, the two lightcurve minima per orbit are expected to have different depths in eclipsing systems. For the non-eclipsing ellipsoidal variables the cause of the difference in the depths of minimum (aside

from the starspot effects) is a combination of mutual irradiation and gravity darkening. In both cases, the differences in the depths of the two minima can be modeled by the addition of a sinusoid at the orbital frequency. Thus, the light curves of many short-period binaries can be described adequately by the first three terms of the expression on the right-hand side of the equation:

$$f(t) \simeq C - E_1 \cos \omega t - E_2 \cos 2\omega t - S \cos(\omega t + \ell) \quad (1)$$

where C is a constant, E_1 and E_2 are the amplitudes that describe the orbital lightcurve of the binary, and S is the starspot amplitude (discussed below). In this expression, the time t is taken with respect to an origin at the primary light-curve minimum, hence the choice of negative cosine functions. The constant C has a value near unity, given that it accounts for the normalized mean flux from the binary. The final term, which we explain next, describes the effect of a starspot or group of spots.

In the simplest form of the model posited in the Tran et al. (2013) paper, the anticorrelated $O - C$ curves result from a starspot that moves slowly around one of the stars. More generally, the $O - C$ effects may result from the combined effects of a number of spots on one or both stars. Whether the effects are due to one or multiple spots is not of critical significance for the analyses presented below; as long as their combined effect produces a sinusoidal modulation at ωt , the mathematical model in Eqn. (1) should be sufficient. The frequency of the motion of the spot is always close to that of the orbital motion, i.e., the star must nearly corotate with the orbit as is expected in very short period binaries. Empirically, the variations due to starspots typically show up in Fourier transforms of flux lightcurves primarily at or very close to the stellar rotation frequency, with progressively less and less power at higher harmonics (see, e.g., Rappaport et al. 2014). In the lightcurve model given by Eqn. (1) we assume that the starspot amplitude at $2\omega t$ is much smaller than the lightcurve amplitude E_2 (typically dominant in very short period binaries) and can therefore be neglected; however, this remains to be verified empirically in this work. We therefore represent the contribution of the starspot to the orbital lightcurve by the $S \cos(\omega t + \ell)$ term in Eqn. (1), where ℓ denotes the longitude of the starspot.

Several additional comments about the spot term in Eqn. (1) are in order. First, this term assumes that the spot is visible around the entire orbit. Roughly speaking, this is only true for spots that are located at places on the star such that $i + \alpha < 90^\circ$, where i is the orbital inclination and α is the colatitude (defined as the complement of the latitude) of the spot, assuming that the spot is located on the hemisphere centered on the $\alpha = 0$ pole (Tran et al. 2013). As was argued in Tran et al. (2013), empirically it appears that this criterion is largely met in those systems where the $O - C$ curves are clearly anticorrelated. Second, the zero of longitude is defined so that it contains the line joining the two stellar centers (near the inner Lagrange point). Third, the sign of the spot term assumes that spots are on the farther star at lightcurve minimum. If the spot is on the nearer star, the sign of the coefficient must be interpreted accordingly. Finally, if the starspot moves in longitude uniformly with time, due to differential stellar rotation or due to imperfectly synchronized stellar rotations, then ℓ will vary linearly

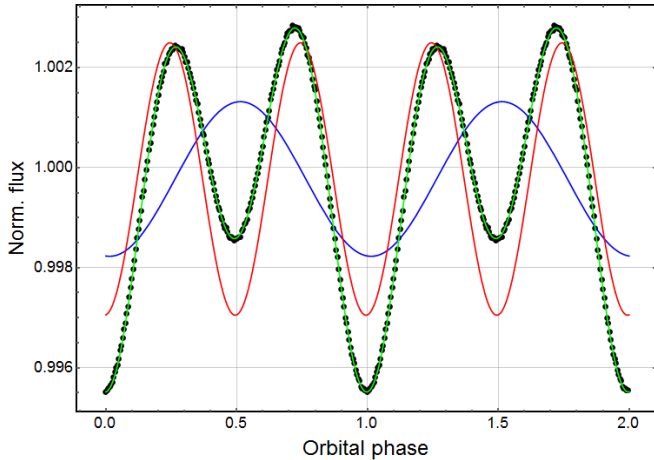


Figure 2. Folded lightcurve for KIC 9002076 (black points) with a fit to a function given by Eqn. (1) with S set equal to zero (i.e. no average contribution from star spots). The blue, red, and green curves show the ωt and $2\omega t$ terms as well as their sum, respectively, where ω is the orbital frequency. Phase zero is taken to be at the primary minimum in the folded light curve. Evidently, when spot behavior is taken out of the picture, the remaining terms—one sinusoid at the binary frequency ω , one at 2ω , and a constant—in Eqn. (1) are sufficient to describe the lightcurve quite accurately.

with time. Wandering of the spot on the stellar surface may produce non-periodic variations in time.

We also note that a bimodal starspot distribution in longitude on one of the stars could introduce a signal at twice the orbital frequency, potentially contributing to, and interfering with, the $\cos 2\omega t$ term in Eqn. (1). While the Fourier harmonics of starspots do tend to fall quickly with frequency (see, e.g., Rappaport et al. 2014), this is a potentially important effect to watch for. Empirically, however, in this work we do not typically find an important time-varying component to the $\cos 2\omega t$ term.

We demonstrate how well the first three terms of the expression in Eqn. (1) can characterize the basic orbital light curve by fitting them to the folded light curve for one of the short-period binaries in this study, KIC 9002076 (see Fig. 2). The process of folding the data tends to average out the starspot behavior, because ℓ varies as the spot migrates (as we show in this work) and thus generally takes on a wide range of values over a long time interval. Figure 2 displays the folded light curve for KIC 9002076 which has (i) very low amplitude modulations, and (ii) two different light curve minima whose depths differ by roughly a factor of two. The fitted curves show the combined contributions of the first three terms in Eqn. (1). As can be seen, the sum of the three terms fits the overall folded lightcurve extremely well.

3.2. The Spot Term

We next examine how well the expression on the right in Eqn. (1), including and especially the $S \cos(\omega t + \ell)$ term, can fit the flux data from a contact binary with migrating spots. If we assume that the value of ℓ in Eqn. (1) does not change rapidly, we may take it to be a constant for short time intervals. In that case we can add the two terms at frequency ω in Eqn. (1) and write it as:

$$f(t) \simeq C - a_1 \cos(\omega t + \phi_1) - a_2 \cos(2\omega t + \phi_2) \quad (2)$$

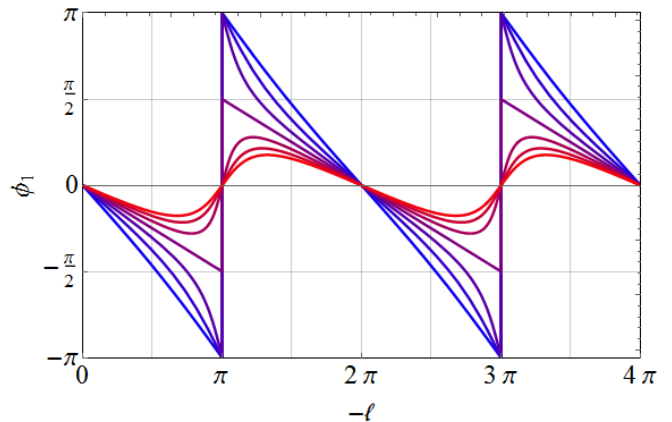
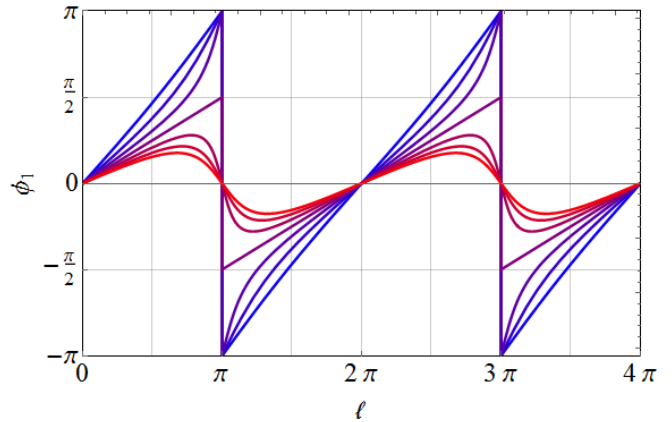


Figure 3. A plot of ϕ_1 as given by Eqn. (4) for several values of S/E_1 , from 0.5 (red) to 10 (blue). This ratio is effectively the ratio of the spot amplitude to the difference between primary and secondary minima depths. The upper plot shows ϕ_1 as ℓ increases with time, while the lower plot shows the shape of ϕ_1 if ℓ is instead a decreasing function of time. Notice that if S/E_1 is large (bluer curve), then ϕ_1 behaves more linearly, with phase wrapping; if S/E_1 is small, ϕ_1 varies almost sinusoidally, with much smaller (and better defined) amplitude. Nonetheless, whether the phase curve exhibits a slow rise followed by a steeper decline, or vice versa, indicates whether the spot motion is prograde or retrograde.

where, as above, t is the time relative to the time of a primary minimum, and therefore ϕ_2 , which we have included for robustness of the fit, should remain near zero. While a_2 is simply equal to E_2 , the amplitude a_1 and phase ϕ_1 are related to E_1 , S , and ℓ by

$$a_1 = \sqrt{S^2 + E_1^2 + 2SE_1 \cos \ell} \quad (3)$$

$$\tan \phi_1 = \frac{S \sin \ell}{E_1 + S \cos \ell} \quad (4)$$

In the limit that the starspot amplitude dominates the orbital amplitude at the orbital frequency, i.e. $S \gg E_1$, then $\phi_1 \simeq \ell$. In that case, as the spot moves all the way around the star, ϕ_1 will cycle through a net angle of 2π radians. If instead $E_1 \gg S$, then $\tan \phi_1 \simeq (S/E_1) \sin \ell$, and the value of ϕ_1 will oscillate over an interval much smaller than 2π radians even as ℓ changes by 2π radians. These behaviors are summarized in Figure 3, where we plot ϕ_1 as given in Eqn. (4) for various ratios of S/E_1 .

The results of Tran et al. (2013) showed that the spot longitude, ℓ , varies significantly even if slowly given the

long duration of almost all of the *Kepler* light curves. Therefore we fit the function in Eqn. (2) to successive segments of the data, arbitrarily chosen to be 500 *Kepler* LC samples in duration (~ 10 days, or between ~ 10 and ~ 30 binary orbital periods). The fits are carried out for segments with starting points offset by 100 LC intervals (~ 2 days) with respect to one another. The time variation of the fitted parameters can be used to infer changes in spot longitudes.

The ability of the function in Eqn. (2) to fit 500-LC sample intervals of a light curve that changes quite obviously over longer timescales is demonstrated by results for one of the contact binaries in our study, KIC 11572643. Fig. 4 shows four short segments of the data each separated by ~ 300 days together with the best-fit functions. Even though the relative depths of the minima are clearly different in each segment, the simple model fits rather well and enables the spot phase and amplitude to be extracted.

3.3. Diagnostic Dissection of a Light Curve

Figure 5 illustrates the decomposition of an entire *Kepler* light curve for one of the short-period binaries in our study, KIC 6431545, into various amplitudes and phases as a function of time.

The top panel provides an overview of the *Kepler* lightcurve, including a sense of the overall variation of the peak-to-peak amplitude. The second panel shows the residuals after the best fit for each segment has been subtracted; since we step the data segments that we fit by 100 points each, the residuals for each consecutive series of 100 points are based on a slightly different fit. The results in this panel give a direct sense of the overall performance of the fitting function since the vertical scale has the same range as that of the light curve plot. The next four panels show the best-fit values of the parameters a_2 , ϕ_2 , a_1 , and ϕ_1 (defined as in Eqn. (2)).

The best-fit values of a_2 and ϕ_2 (third and fourth panels) vary very little, indicating that the corresponding $2\omega t$ term remains relatively consistent throughout the light curve. Since this is the dominant term in the description of the orbital contribution to the light curve, this behavior is as expected, assuming (i) there are no external perturbations to the orbit such as those that would be produced by a third body in the system, or (ii) a dominant bimodal starspot distribution in longitude causing unanticipated power in the $\cos 2\omega t$ term. The fitted values of a_1 (fifth panel) indicate the amplitudes of the flux modulations caused by the starspot (over and above the nominal binary lightcurve). Of note in this particular system is that a_1 is largest where the amplitudes of the flux data themselves and the $O-C$ curves (bottom panel) are both also largest. This expected correlation is indeed visible in many of the sources we analyzed.

The sixth panel in Fig. 5 is striking. It shows that ϕ_1 decreases at a nearly steady rate, wrapping around 2π radians presumably in concert with the spot longitude. This behavior indicates that the actual frequency of the spot term is slightly *lower* than the orbital frequency. This would be expected from the variations due to a spot on a star that is rotating at a rate slightly *below* that of the binary orbit. According to this interpretation, the ~ 6.5 cycles of ϕ_1 indicate that the spot circles the star (in a frame of reference rotating with the binary)

just over 6.5 times during the four years of the *Kepler* observations.

It is important to note that the slow drift of ϕ_1 almost certainly arises from the spot being carried around the star as viewed in a reference frame rotating at the orbital frequency. This would occur if the entire star is rotating like a solid body at a rate below or above that of the orbit, i.e., if the rotation of the star with the spot is not synchronized with the orbital motion (i.e., not tidally locked). A second possibility is that the rotation of part of the star, likely the equatorial region, is indeed tidally locked to the orbit, but that there is nevertheless differential rotation so that there is a region at, e.g., a higher stellar latitude that is not rotating at the orbital rate. A third possibility is that the spot migrates in longitude due to another cause, one possibility being a systematically time-varying magnetic field configuration that might drive the location where spots appear. Of course, some combination of these is also possible. In any case, the observed nonuniformities in the drift rate of the spot are likely to be due to motions of the spot relative to the mean motion of the stellar surface at nearby latitudes.

The bottom panel in Fig. 5 shows the $O-C$ curves for the primary (red points) and secondary (black) lightcurve minima.

4. PHASING THE $O-C$ WITH THE ϕ_1 CURVES

Starspot behavior is manifest in both $O-C$ curves and plots of ϕ_1 versus time (as defined above), although there are significant differences. To be specific, the $O-C$ values measure timewise-local (near primary or secondary minimum) spot photometric effects, whereas phase tracking involves fits of entire orbital cycles. Thus, it is natural to check how the two are related.

One way to ascertain whether the $O-C$ and ϕ_1 curves are measuring effects due to the same starspots is to check how the zeros of the ϕ_1 plots (i.e., $\phi_1 = 0$) align with the intersections of the primary and secondary $O-C$ curves.⁴ However, we must first be sure that the meaning of “phase” is identical between the two plots. In the $O-C$ curves, the points of zero deviation for both the primary and secondary minima occur (by symmetry) when the spot is at a stellar longitude $\ell = 0$ or π , which according to Eqn. (4) implies $\phi_1 = \ell$ at that point. Thus, the zeros in the $O-C$ curves should align with values of ϕ_1 equal to 0 or π .

In connection with Eqn. (1), it was noted that $t = 0$ should be set to the time of a primary minimum. If the times of the primary minima are not precisely periodic, there is latitude in the choice of the time origin. Indeed, the choice of the time origin was acknowledged to be approximate in Eqn. (2) by allowing a nonzero value of ϕ_2 . In practice, the overall average value of ϕ_2 was used as a reference to effectively set the time of orbital phase zero, and to thereby also set the zero-point reference for ϕ_1 , i.e., the figures show the values of $\phi_1 - \langle \phi_2 \rangle / 2$ and $\phi_2 - \langle \phi_2 \rangle$ rather than the raw values of ϕ_1 and ϕ_2 .

⁴ The intersections of the primary and secondary $O-C$ curves would occur at zero delay as well, except for any *correlated* behavior between the primary and secondary curves due to extraneous causes.

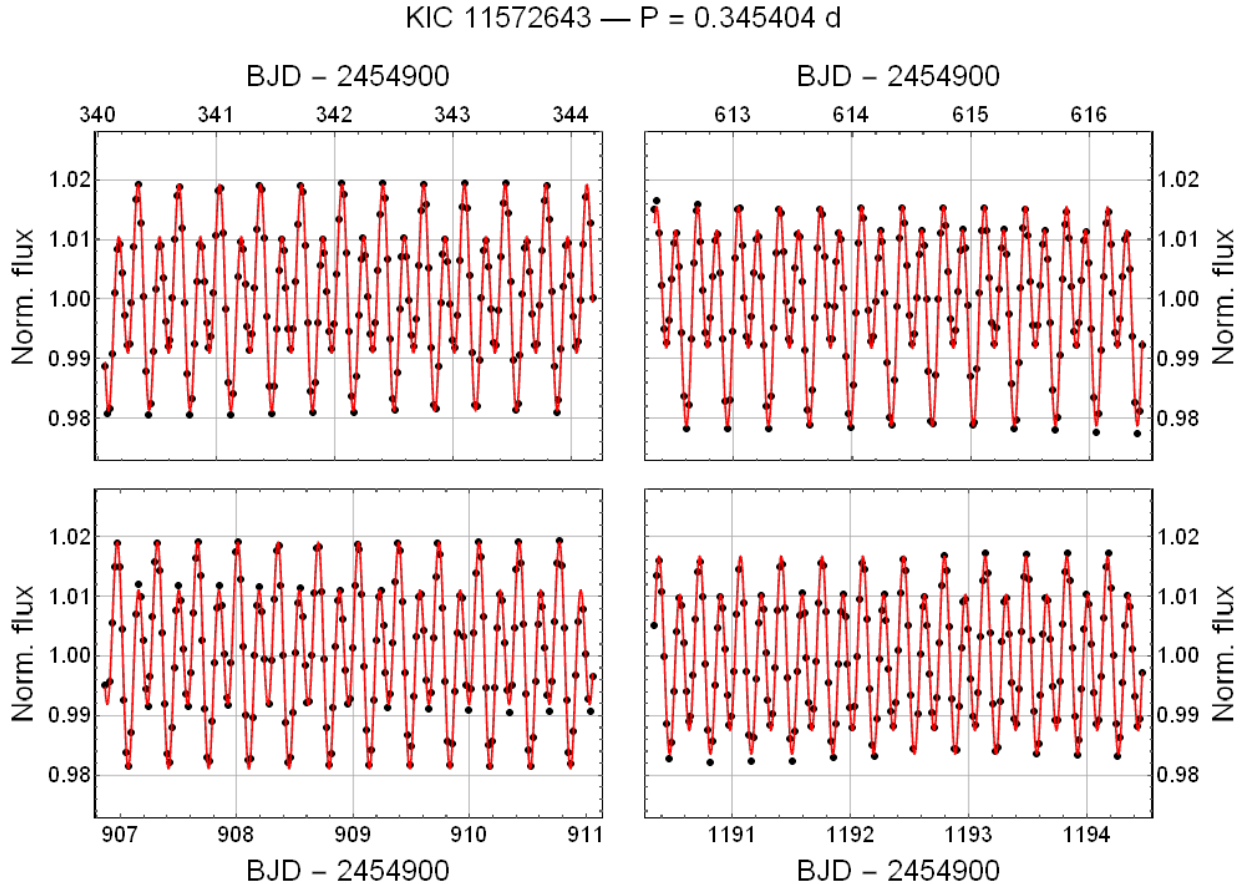


Figure 4. An illustrative example of how well the fitting function given by Eqn. (2) can describe the *Kepler* data for a contact binary with an assumed migrating starspot. Here we show the results for four different segments of the flux data from the binary KIC 11572643. In *each* segment a single value for the spot amplitude and phase is assumed; these parameters do vary from segment-to-segment. The shape of the fitting function (in red) is noticeably different in each segment, presumably due to the changes in spot longitude, but the fit is still excellent in all four segments of data.

4.1. Comparison of $O - C$ and ϕ_1 Curves for a Sample of a Dozen Binaries

From a sample of 414 short-period binaries with anticorrelated $O - C$ curves listed in Table 2 and Appendix A⁵, we selected 12 that had especially well-behaved $O - C$ curves. In Sect. 5 we will present a summary of the $O - C$ periodicities for the entire sample of systems. Here the $O - C$ and ϕ_1 curves for the 12 selected binaries are compared in detail.

Figure 6 shows the $O - C$ and ϕ_1 curves for KIC 7304911, KIC 9713664, and KIC 11572643. In all three cases, the pair of curves shows excellent consistency in the sense that the times when the primary and secondary $O - C$ curves intersect coincide with the times when $\phi_1 = 0$ or π . This is quite compatible with our interpretation that both the $O - C$ behavior and ϕ_1 's cycling through 2π are due to spots drifting slowly in longitude (with respect to a line joining the two stellar centers). Note also that in all three of these cases, ϕ_1 is basically linear modulo 2π —this is because these sources have very similar depths for the primary and secondary lightcurve minima. As a result, E_1 is negligible, and per the discus-

⁵ Tran et al. (2013) first identified 390 of this set of short-period binaries with anticorrelated $O - C$ curves.

Table 1
Spot Movement Behavior Among
414 Contact Binaries

Classification	Percentage
Prograde Motion	13.0
Retrograde Motion	34.3
Small Phase Changes	45.6
Erratic Behavior	7.2

sion in Sect. 3.2, $\phi_1 = \ell$, meaning that it directly tracks the spot longitude.

In all three cases shown here, as is true for some 34% of the 414 systems we investigated (see Table 2 and Appendix A), the phases decrease essentially monotonically with time (modulo 2π), which is indicative of a slowly counter-rotating spot (i.e., one with retrograde motion). About 13% of the systems instead exhibited ϕ_1 *increasing* with time (i.e., prograde motion), while the remaining 53% displayed either erratically moving or relatively stationary phases (the latter being those that did not wrap by 2π more than once over the entire duration of the light curve). The percentages of systems with different spot rotational behaviors are summarized in Table 1.

The $O - C$ and ϕ_1 curves for KIC 9934052, KIC

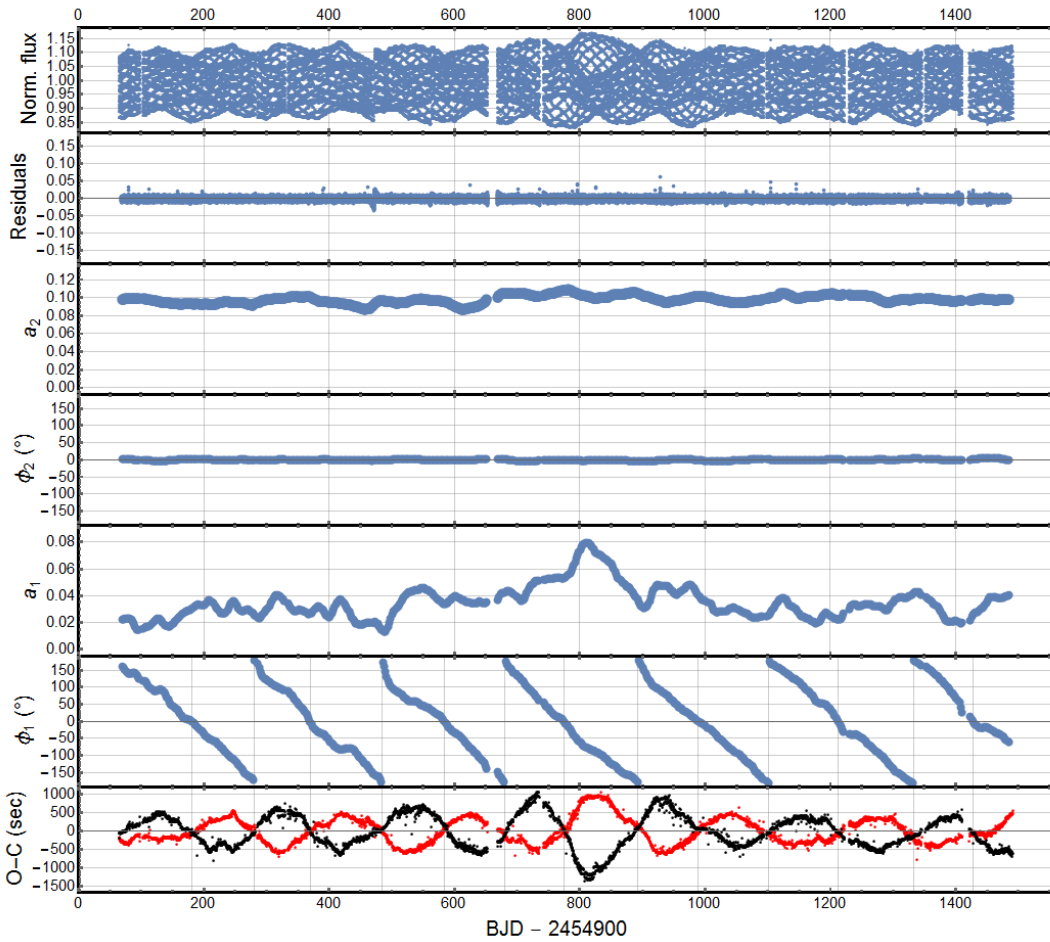
KIC 6431545 — $P = 0.316834$ d

Figure 5. Parameters determined by fits of a function of the form given by Eqn. (2) to 500-point segments (which are then stepped by 100 points) of the light curve of the contact binary KIC 6431545. The panels are as follows (top to bottom): the normalized *Kepler* flux data; the residuals after the fits have been subtracted from the flux data; individual fitted parameters a_2 , ϕ_2 , a_1 , and ϕ_1 ; and the $O - C$ curve for the primary minimum (red points) and secondary minima (black points). The vertical gridlines in the bottom two panels are placed at the locations where ϕ_1 crosses 0 and π , showing that these locations match with those where the $O - C$ curves intersect each other. Note that the flux data (top panel) exhibit a Moiré pattern, i.e., a beat between the binary period and the *Kepler* long-cadence sampling time.

8956957, and KIC 9957411 are displayed in Fig. 7. These three systems clearly exhibit spot motions that are substantially more rapid than those of the examples shown in Fig. 6. The ϕ_1 curves wrap around by an angle of 2π radians substantially more times in 1400 days than for any of the systems shown in Fig. 6. All three of these ϕ_1 curves contain intervals, aligned with intervals of low-amplitude $O - C$ activity, in which ϕ_1 fails to wrap around by 2π and instead oscillates. Both of these behaviors, i.e., regions of low-amplitude $O - C$ curves and failure of ϕ_1 to wrap, indicate weak starspots, the former from our discussion in Sect. 3.2 and the latter from Tran et al. (2013).

Oscillatory (non-wrapping) ϕ_1 behavior is seen in the results for KIC 3342425, KIC 4464999, and KIC 9002076 (see Fig. 8). From this, we conclude, again based on the discussion in Sect. 3.2, that the spot amplitude S is comparable to, or smaller than, the amplitude E_1 (see Eqn. (4)), and therefore the variation of ϕ_1 is limited to a range of only $\sim \pm S/E_1$ radians. Indeed, among the systems we have studied, those where the depths of the

two light-curve minima are significantly different and E_1 is non-negligible tend to have low-amplitude oscillating ϕ_1 curves. In spite of their small amplitudes, the phase ϕ_1 of the spots can be tracked rather well (with zeros still matching up quite well with intersections in the primary and secondary $O - C$ curves), and we see clearly that the phase curves consistently have sharper rises followed by slower falls. This provides an indication, in the absence of wrapping, of spots that rotate more slowly than the orbit (see Fig. 3).

We present the final three examples in Fig. 9 primarily to show that there do exist binaries with spots that are apparently rotating *faster* than the orbit; otherwise they share characteristics that are exhibited by the other 9 examples. The overall ratio of clearly prograde systems, such as those in Fig. 9, to clearly retrograde systems is $\sim 4:10$.

To verify that a system where ϕ_1 varies over only a small range of angles (see, e.g., Fig. 8) is, in fact, consistent with our model, the analysis must be redone after the $E_1 \cos \omega t$ variation has been removed from the light

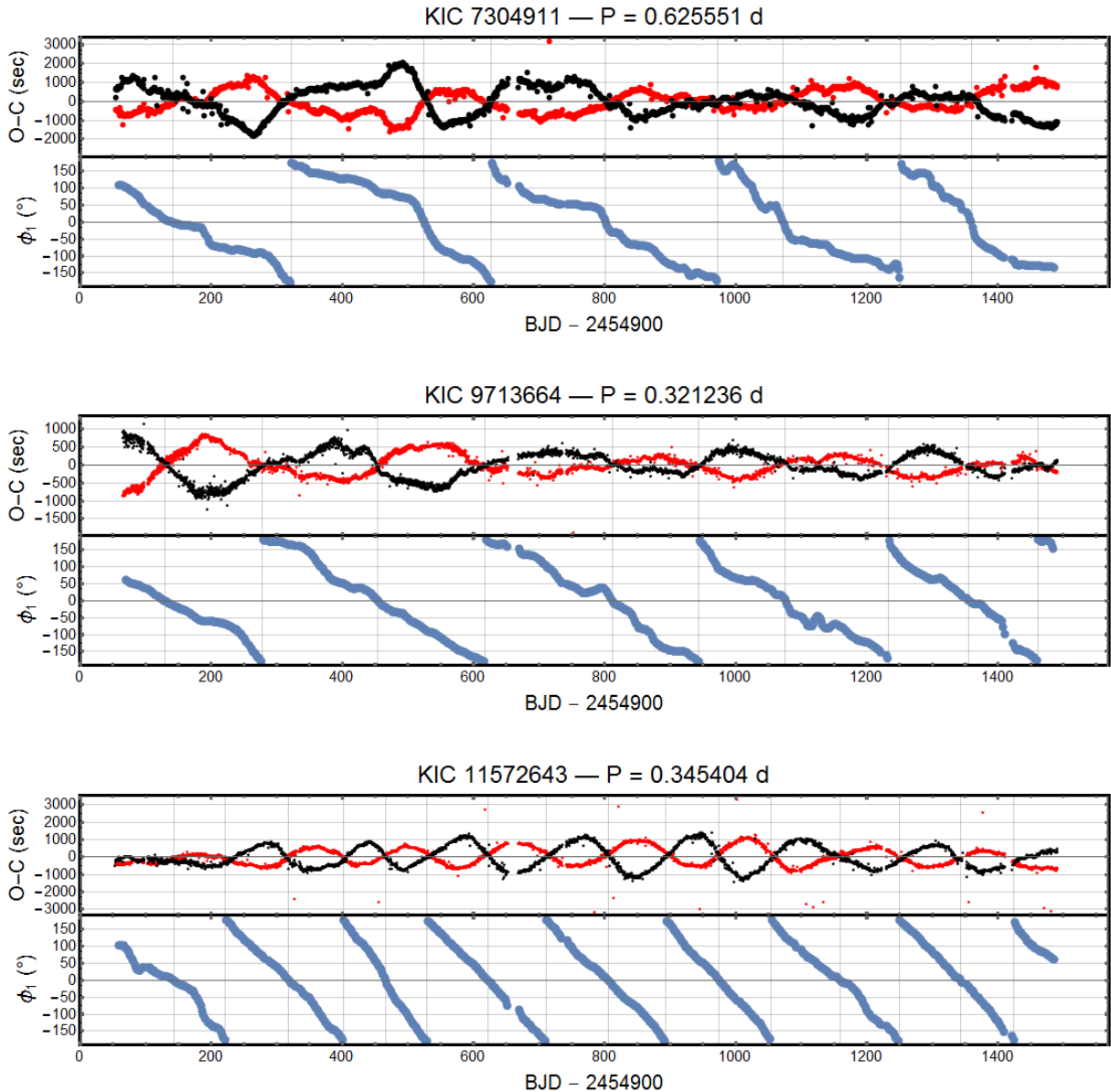


Figure 6. The first 3 of 12 examples of binaries for which we compare the $O - C$ and ϕ_1 curves (KIC 7304911, KIC 9713664, and KIC 11572643). For each binary, the upper plot shows the $O - C$ curves for the primary (red) and secondary (black) minima. The lower plot is of ϕ_1 , as defined in Eqn. (2); we believe ϕ_1 tracks the location of a starspot (or group of starspots) on one of the binary stars. The KIC number and the orbital period are given at the top of the plots for each system. The vertical gridlines are placed where the plot of ϕ_1 intersects 0 or π . (The zero-point reference for ϕ_1 is taken to be the mean value of $\phi_2/2$, when averaged over all the *Kepler* data.) Note how well the $O - C$ intersections agree with these gridlines – strongly indicating that both types of curves are tracking the effect of the same phenomenon in the lightcurves, namely spots.

curve. This is straightforward to accomplish. We simply subtract off an approximation to the $E_1 \cos \omega t$ term from the data, having taken E_1 to be the value of a_1 from the fit of Eqn. (2) to the *entire data set*. This is equivalent to fitting the folded lightcurve, as in Fig. 2, and, in the process, this tends to average out the spot contribution as noted above. Thus subtracting this fitted term removes the difference between the depths of the primary and secondary minima. We apply this method to KIC 9002076; the results are shown in Fig. 10. The top panel is a copy of the bottom panel in Fig. 8, where no $E_1 \cos \omega t$ term was subtracted before the phase fitting was done. The bottom panel shows the corresponding plot of ϕ_1 vs. time

made after the $E_1 \cos \omega t$ term was subtracted from the light curve. Note that after the subtraction, ϕ_1 wraps around 2π radians many times.

5. SUMMARY RESULTS FOR 414 BINARIES WITH ANTICORRELATED $O - C$ CURVES

The $O - C$ curves contain information about the timescales of the motions of the spots around the stars in the rotating frames of the binaries. For the estimation of the timescales, it is best to use the difference of the primary and secondary $O - C$ curves for each system so as to magnify the anticorrelated effects and eliminate correlated ones. Simple interpolation was used to obtain the difference curves. Then, the autocorrelation function,

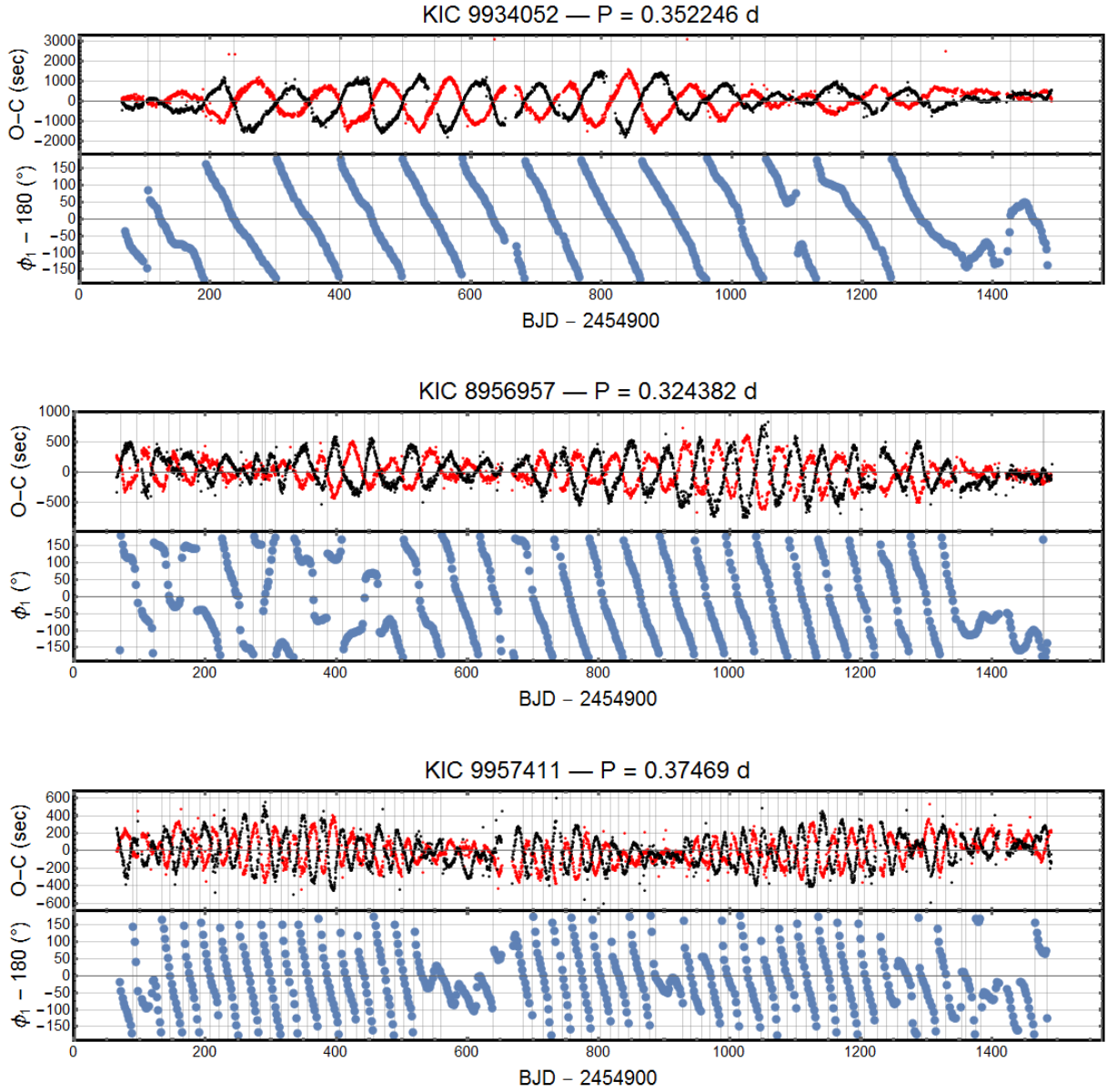


Figure 7. The second group of 3 of 12 examples of binaries displayed similarly to Fig. 6. The binaries chosen for this figure exhibit more rapid rates of change in ϕ_1 than those shown in Fig. 6, which may be taken to indicate higher speeds of spot motion in longitude (ϕ_1 is the spot longitude relative to a line joining the stellar centers). The ϕ_1 curves for KIC 9934052, KIC 8956957, and KIC 9957411 wrap around by an angle of 2π radians approximately 13, 21, and 31 times during the *Kepler* observations, corresponding to spots migrating all the way around their host star numerous times. There are several intervals in each of these ϕ_1 curves where the phase ceases to wrap around in a regular fashion—these correspond to intervals of weak (low-amplitude) spot behavior and correspondingly low amplitudes in the $O - C$ curves. The ϕ_1 curves for the top and bottom panels are presented as “ $\phi_1 - 180$ ” in order to keep visible any clearly oscillatory or pseudo-oscillatory behavior. We do likewise in the rest of this paper for any other binaries for which this presents a clearer picture.

$ACF(t)$, was computed for each $O - C$ difference series in order to extract the underlying periodicities (see, e.g., McQuillan et al. 2013). To accomplish this, we fit the autocorrelations over delays of 0 to 400 days with the somewhat arbitrary analytic function

$$ACF(t) \simeq \frac{A \cos Bt}{(t + 1 \text{ d})^C} \quad (5)$$

with constants A , B , and C . The characteristic starspot migration period is then taken to be $P_{\text{mig}} = 2\pi/B$.⁶ This

⁶ The spot migration period is approximately the modulation period in the $O - C$ curve. See Eqn. (7) in Tran et al. (2013)

is the time it takes a spot to move completely around the host star in the reference frame of the rotating binary. If P_s is defined as the spot rotation period as viewed from inertial space, then these two periods are related to the binary orbital period, P_{orb} by:

$$P_{\text{mig}} = \frac{P_{\text{orb}} P_s}{|P_{\text{orb}} - P_s|} \simeq \frac{P_{\text{orb}}}{|1 - P_s/P_{\text{orb}}|} \quad (6)$$

as long as P_s and P_{orb} are close in numerical value. The absolute value must be taken when $P_s > P_{\text{orb}}$ in order to

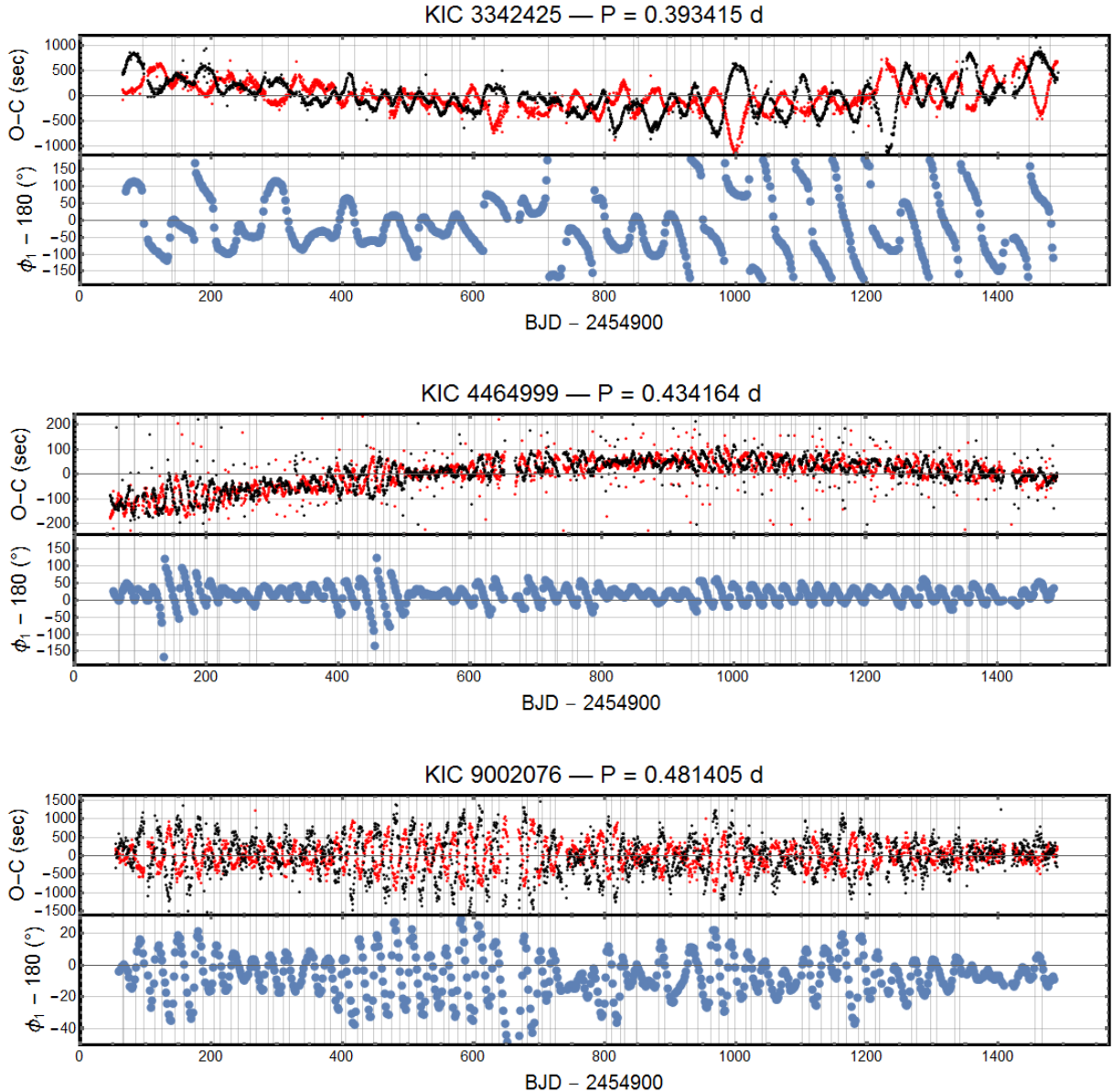


Figure 8. The third group of 3 of 12 examples of binaries displayed similarly to Fig. 6. These three binaries (KIC 3342425, KIC 4464999, and KIC 9002076) demonstrate the effect of having a spot amplitude that is comparable to, or smaller than, the difference between the depths of the primary and secondary minima (see Eqn. (4) and the accompanying discussion in Sect. 3.2). In these cases, ϕ_1 oscillates around π (we present $\phi_1 - \pi$ to make the oscillations clear), rather than behaving linearly modulo 2π . Of course, ϕ_1 could oscillate around 0 instead—the offset by π is only a question of which star the spot is on. Notice that the phase curves all consistently have steep rises followed by slower declines, indicative of spots that rotate more slowly than the orbit. Also note that the vertical scale on the ϕ_1 plot for KIC 9002076 is expanded to better show the oscillations.

keep P_{mig} positive. We further define the quantity κ by

$$\kappa \equiv \frac{P_s}{P_{\text{orb}}} - 1 \quad (7)$$

and its absolute value is then given by

$$|\kappa| = \frac{P_{\text{orb}}}{P_{\text{mig}}}. \quad (8)$$

Based on sunspot behavior, a simple model for the differential rotation of spotted stars has been adopted for this problem (e.g. Hall & Busby 1990; Kalimeris 2002)

such that

$$\kappa' \equiv \frac{P - P_{\text{eq}}}{P_{\text{eq}}} = k \cos^2 \alpha$$

where P and P_{eq} are the rotation periods of the star at colatitude α (as defined above) and at the equator, respectively. The differential rotation constant, k , in our application, may be positive or negative or zero. In the Sun, k is positive and κ describes the increasing nature of the spot rotation period with increasing latitude (decreasing colatitude). In our close binary problem, the details of any differential rotation and the exact cause of the apparent spot motion are not known, so we simply use κ as the parameter to be measured; k and κ may

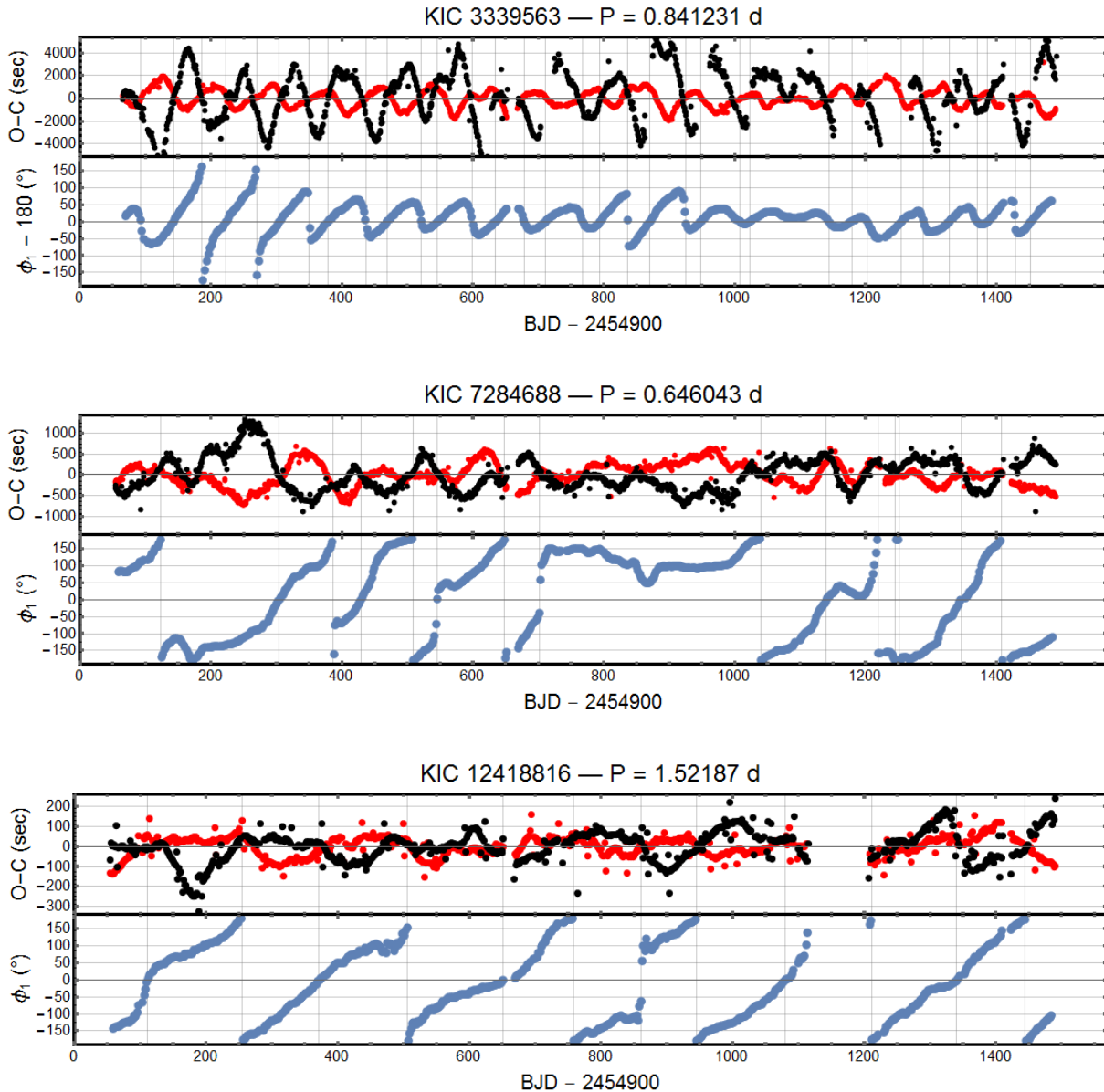


Figure 9. The fourth group of 3 of 12 examples of binaries displayed similarly to Fig. 6. The three binaries shown here (KIC 3339563, KIC 7284688, and KIC 12418816) are all examples for which ϕ_1 is predominantly increasing (aside from wrapping around by 2π) with time, i.e., the differential rotation of the spots is prograde with respect to the orbit. In the case of KIC 3339563 this behavior is clear because of the slow rises and steep falls during the oscillatory portion of the ϕ_1 curve which dominates most of the data train, as well as in the shorter wrapping (non-oscillatory) interval near the start. In all other respects, these curves are similar to the other 9 sources as shown in Figs. 6, 7, and 8.

have either sign. In relating k to κ , we note that the quantity $\cos \alpha$ is likely to be $\gtrsim 0.7$ or $\cos^2 \alpha \gtrsim 0.5$. This results from the various constraints put forth by Tran et al. (2013) for the orbital inclination and spot colatitude in order to accommodate the observed anticorrelated $O - C$ curves. Stated simply, this results from the requirements that $i \gtrsim 40^\circ$ and $i + \alpha < 90^\circ$, and therefore $\alpha \lesssim 50^\circ$.

We utilized the fits of Eqn. (5) to the autocorrelation functions computed for the $O - C$ curves of all of the 414 binaries in this study. From the B coefficient for each system, we evaluated a representative value for P_{mig} . This value was then used to compute $|\kappa|$. Some 390 of the 414 systems yielded meaningfully measured values for κ ; the

distribution of $|\kappa|$ for this sample is shown in Fig. 11. We find that most systems have values of $|\kappa|$ that lie between 0.0003 and 0.005, but with another $\sim 20\%$ having values out to $|\kappa| \simeq 0.03$.

Reinhold et al. (2013) have carried out an extensive study of differential rotation in 40,660 active *Kepler* stars⁷. In some 18,600 of these stars they find two or more close rotation periods which they take as evidence for differential rotation and which they then use to derive limits on the differential rotation properties. Their

⁷ These stars are mostly either single or in non-interacting binaries. Moreover, we note that the rotational periods covered in that study are limited to $P_{\text{rot}} \gtrsim 0.5$ days, so not quite as short as the binary periods we are investigating.

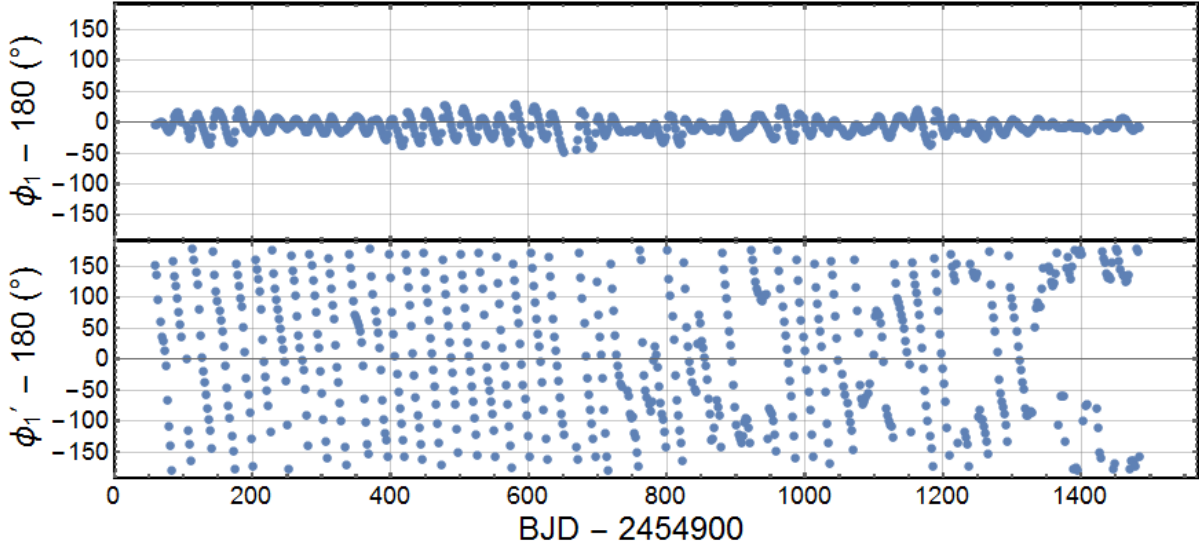
KIC 9002076 — $P = 0.481405$ d

Figure 10. Plots of ϕ_1 before (above) and after (below) subtracting an overall $(a_1) \cos \omega t$ term from the lightcurve for KIC 9002076. (To mark its distinctness from ϕ_1 , we label the quantity in the lower figure ϕ_1' .) By fitting Eqn. (2) to the whole data series at once, the spot behavior averages out, as it does in the folded light curve shown in Fig. 2. Then, subtracting the fitted $(a_1) \cos \omega t$ term is equivalent to subtracting the $E_1 \cos \omega t$ term in Eqn. (1). There are no significant differences between the depths of the primary and secondary minima in the resulting light curve, so spot behavior is more clearly picked up by new, segment-by-segment fits using Eqn. (2).

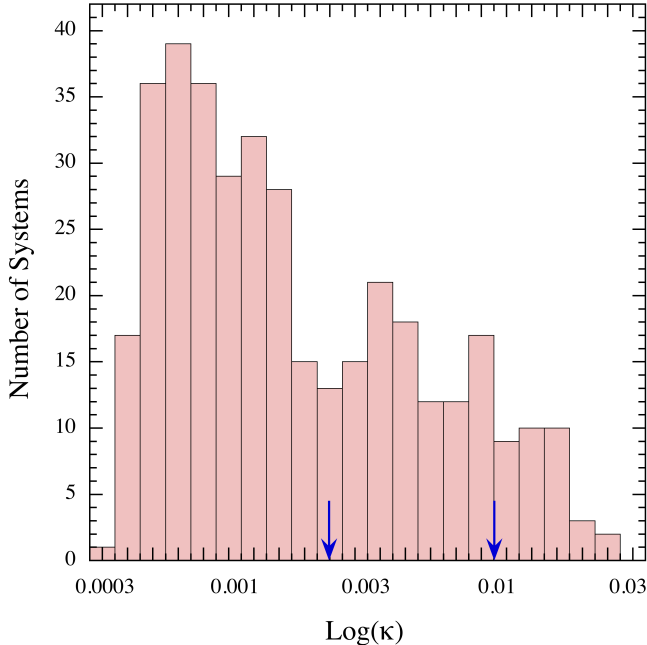


Figure 11. A histogram of our calculated differential rotation coefficient $|\kappa|$ (as defined in Eqn. 8) for each of 390 contact binaries with anticorrelated primary and secondary $O-C$ curves. The bins in $|\kappa|$ are spaced logarithmically. Plots of all the $O-C$ curves can be found in Appendix A. The signs of spot rotation frequency with respect to the binary orbit are not defined by the $O-C$ curves, but we summarize the prograde, retrograde, and ‘others’ categories in Table 1. The blue vertical arrows mark the range of values of k from Reinhold et al. (2013) for single stars with T_{eff} in the range of 4800 K to 6500 K (derived from Eqn. (9) after multiplying by 0.37 d for the median period of our binaries; see Fig. 1).

Fig. 15 summarizes the measured values of horizontal shear differential rotation parameter $\Delta\Omega \equiv \Omega_{\text{eq}} - \Omega$, which is defined as the difference in rotation frequency between the equator and the pole. For stars hotter than ~ 6400 K, values of $\Delta\Omega$ are often found to exceed 0.2 rad d^{-1} . However, for stars with T_{eff} in the range of 4800 K to 6400 K, which covers most of the range we are studying here (see Fig. 12), $\Delta\Omega$ spans values of ~ 0.035 to $\sim 0.2 \text{ rad d}^{-1}$. This translates to our fractional differential rotation parameter, κ as:

$$\kappa \equiv \frac{\Delta\Omega}{\Omega_{\text{eq}}} \simeq 0.0055 \rightarrow 0.03 \times P(\text{days}), \quad (9)$$

where $P = 2\pi/\Omega_{\text{eq}}$. The range given by Eqn. (9), after multiplying by the median orbital period in our sample of 0.37 days (see Fig. 1), is $\kappa \simeq 0.002 \rightarrow 0.01$, well within the range of values shown in Fig. 11, though centered on a value that is about a factor of three higher than the mean of the histogram in Fig. 11. This modest difference might lead to the speculation that the differential rotation of many of the stars in tight binaries is less pronounced than that of single stars or wide binary systems.

In direct regard to close binary systems, Hill et al. (2014) have measured the star spot rotation on the donor star in the cataclysmic variable star AE Aqr with an orbital period of 0.411 days. The observations were made via Roche tomography of the K4V donor star in the system. They find from two observations separated by 9 days, that there are two distinct bands of spots (at latitudes of 22° and 43°) that have ‘lap times’ (referred to in our work as P_{mig}) of 262 and 269 days. This corresponds to $|\kappa| \sim 0.0016$, quite near the center of the distribution in Fig. 11 before taking into account the $\cos^2 \alpha$ factor, but toward the lower end of the distribution after taking it

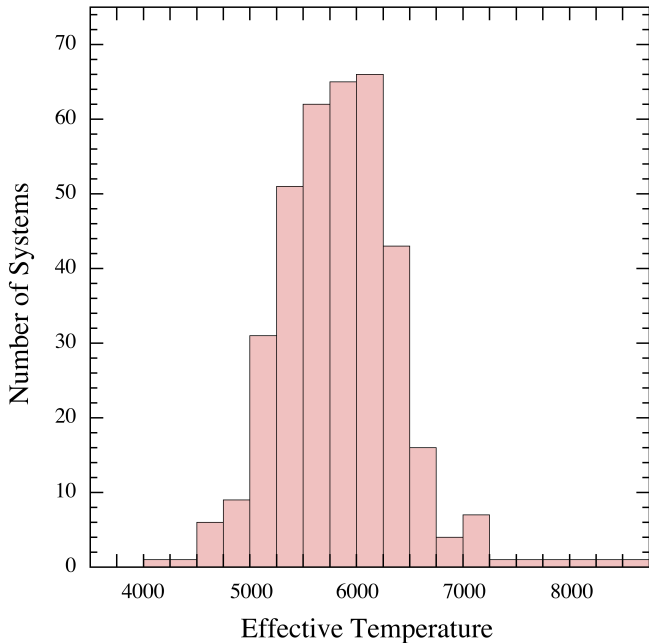


Figure 12. A histogram of the effective (i.e., composite) temperature (T_{eff} taken from the KIC) for each of 390 contact binaries with anticorrelated primary and secondary $O - C$ curves that yielded measurable values of κ . The vast majority of the systems are characterized by a value of T_{eff} in the range 5000 to 6500 K.

into account. By contrast, Hussain et al. (2006) showed that the pre-cataclysmic variable star V471 Tau, with an orbital period of 0.521 days, has no measurable $\Delta\Omega$ with a constraint of $\lesssim 6 \text{ mrad d}^{-1}$. This translates according to Eqn. (9) to $\kappa \lesssim 5 \times 10^{-4}$. Such a value corresponds to the lower limit on what we are able to measure in the current work. However, these two examples can serve to indicate the importance of measuring a large sample of close binaries before drawing any sweeping conclusions.

6. FINDING TRIPLES WITH ϕ_2

We noted earlier that we expect ϕ_2 to remain constant *assuming no external perturbations* to the binary orbit. Therefore a systematically varying ϕ_2 can allow us to infer the presence of an external perturbation to the binary, such as a third body. In Fig. 13, we present the example of KIC 5478466, where the *correlated* behavior in its $O - C$ curve is characteristic of a binary that is actually part of a triple system (see Conroy et al. 2013). Note that in Fig. 13, ϕ_2 exhibits the same variation, but with the opposite sign as that in the $O - C$ curve (as can be shown formally from the respective definitions of $O - C$ and ϕ_1). The parameters we find for this triple are the period of the third body’s orbit $P_{\text{trip}} = 740.5 \pm 2$ days (763 ± 72 days); the eccentricity of its orbit $e = 0.499 \pm 0.03$ (0.459 ± 0.003), and the projected semimajor axis of the CM of the binary system in its orbit about the third star $a_{\text{bin}} \sin i = 210.7 \pm 1.5$ sec (206 ± 13 sec), where the values in parentheses are those reported by Conroy et al. (2013). Thus it seems that we can also use the ϕ_2 curves to search for new triple star systems (see Rappaport et al. 2013), without having the anticorrelated behavior of the $O - C$ curves making the correlated behavior more difficult to discern.

In this way, we were able to identify 39 triple systems

where we infer the presence of a third body in the system via Roemer delays inscribed on the ϕ_2 curves. All but four of these had been previously reported by Rappaport et al. (2013) and Conroy et al. (2013).

7. SUMMARY AND CONCLUSIONS

Tran et al. (2013) presented a spot model involving stellar differential rotation to explain anticorrelated oscillations in the $O - C$ curves for the times of primary and secondary minima in 32 short-period *Kepler* binaries. In this work, we used similar assumptions to those in that model to track explicitly the movement of spots around their host stars for 414 very short-period *Kepler* binaries with anticorrelated $O - C$ curves (see Appendix A and Fig. 11). The success of our phasing analysis further validates the model involving spots that do not quite corotate with the binary orbit.

We found that about $\sim 34\%$ of the binaries exhibited spots moving in a retrograde sense with respect to the binary orbit, while $\sim 13\%$ exhibited spots moving in a prograde manner. The remaining binaries had either erratically moving spots—which could rather be caused by the appearance or disappearance of spots—or spots that did not move much in stellar longitude (see also Tran et al. 2013).

There are at least three plausible causes that could result in this spot motion relative to the binary. The first is that the entire body of the spotted star could be rotating asynchronously with respect to the orbit (i.e., not tidally locked stars). The second is that the equatorial zone, for example, of the star is synchronized, but that higher latitudes are rotating at different rates. In the latter case, individual stars (at the very least those that carry a spot) may be rotating more slowly (34%) or more rapidly (13%) with increasing stellar latitude. A third possibility is that the spot can migrate in longitude due a physical effect such as a systematically time-varying magnetic field configuration that might drive the location where spots form. The observations could, of course, also be explained by a combination of asynchronously rotating stars, differential rotation in individual stars, and spot migration. Finally, we note that the *jitter* that exists in nearly all of our ϕ_1 curves is too large to be due solely to changes in the angular velocity of the stars (due to insufficient torques on the star), so asynchronous stellar rotation cannot be a sufficient explanation.

Assuming that the explanation for the moving spots is dominated by differential stellar rotation, we can estimate the distribution of differential rotation values for 390 of the 414 binaries in this study. We actually computed the distribution of a parameter $|\kappa|$ which is formally defined as $P_{\text{orb}}/P_{\text{mig}}$ (see Eqn. 8) that can be related to the more standard differential rotation constant by $\kappa = k \cos^2 \alpha$, where α is the spot colatitude. We showed that since $\cos^2 \alpha$ is likely within a factor of 2 of unity in the systems of interest, $|\kappa|$ can serve as a meaningful proxy for k . We find that $|\kappa|$ mostly ranges between 0.0003 and 0.005, but a modest fraction ($\sim 20\%$) of the fitted values range up to $\kappa \simeq 0.03$. The values of k found for single stars and non-interacting binaries (Reinhold et al. 2013; Eqn. 9) are solidly in this range of values of $|\kappa|$ after multiplying in Eqn. (9) by 0.37 days which is the median orbital period of our sample. The Reinhold et al. (2013) values of k are then only modestly shifted

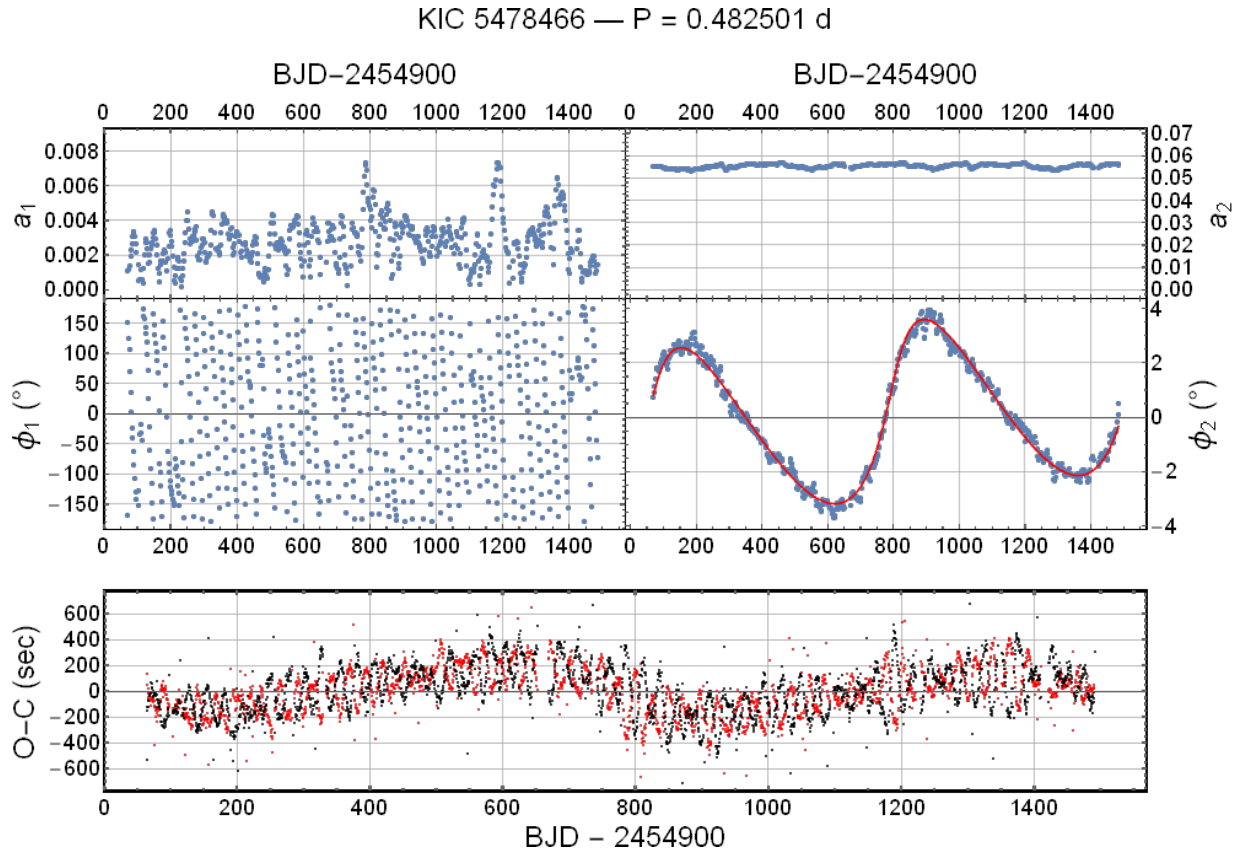


Figure 13. The fitted parameters for KIC 5478466, as well as its $O - C$ curve, plotted as a function of time. The ϕ_2 curve has the characteristic shape (but of opposite sign and twice the amplitude) of an $O - C$ curve dominated by a classical Roemer delay induced by a third star in the system. The superimposed plot (red) is a best-fit eccentric Keplerian orbit.

toward the higher end of our $|\kappa|$ distribution, by a factor of ~ 3 (Fig. 11). This suggests two things. First, the rotation of *observed* spots in our sample of close binaries most likely is *not generally completely synchronized* with the orbital motion. Second, the difference between the spot rotation rate and the orbital rate is often smaller, i.e., by a factor of ~ 3 on average, than would be typical of simple differential stellar rotation in isolated stars.

Another byproduct of our analysis is a new method of looking for third bodies among contact binaries. Just as one would search for correlated behavior in $O - C$ curves that would be indicative of a third body, one can use ϕ_2 curves like those that we generated for our 414 contact binaries. With the ϕ_2 curves, though, there is the additional benefit of not having anticorrelated effects that can obscure the relevant, long-term correlated effects, which often have a similar amplitude scale.

We thank Tamás Borkovits, Katalin Olah, and Slavek Rucinski for very useful discussions, and an anonymous referee who made a number of helpful suggestions – including the possibility of spot migration due to time-varying magnetic field configurations. The authors are grateful to the *Kepler* Eclipsing Binary Team for generating the catalog of eclipsing binaries utilized in this work. We also thank Roberto Sanchis-Ojeda for his help in preparing the stitched data sets. B.C.’s work was performed under a contract with the California Institute of Technology funded by NASA through the Sagan Fellow-

ship Program.

REFERENCES

- Batalha, N.M., Rowe, J.F., Bryson, S.T., et al. 2013, *ApJS*, 204, 24
- Borkovits, T., Elkhateeb, M. M., Csizmadia, Sz., Nuspl, J., Bíró, I. B., Hegedüs, T., & Csorvási, R. 2005, *A&A*, 441, 1087
- Borucki, W. J., Koch, D., Basri, G., et al. 2010, *Science*, 327, 977
- Caldwell, D.A., Kolodziejczak, J.J., Van Cleve, J.E., et al. 2010, *ApJ*, 713, L92
- Conroy, K. E., Prša, A., Stassun, K. G., Orosz, J. A., Fabrycky, D. C., & Welsh, W. F. 2014, *AJ*, 147, 45]
- Geske, M. T., Gettel, S. J., & McKay, T. A. 2006, *AJ*, 131, 633
- Jimenez, A., & Garcia-Pelayo, J.M. 1983, *ApJS*, 92, 203
- Hall, D. S., & Busby, M. R. 1990, in *Active Close Binaries*, ed. C. Ibanoglu (Dordrecht: Kluwer), 377
- Jenkins, J.M., Chandrasekaran, H., McCauliff, S.D., et al. 2010a, *Society of Photo-Optical Instrumentation Engineers (SPIE) Conference Series*, Vol. 7740
- Jenkins, J.M., Caldwell, D.A., Chandrasekaran, H., et al. 2010b, *ApJ*, 713, L87
- Kalimeris, A., Rovithis-Livaniou, H., & Rovithis, P. 2002, *A&A*, 387, 969
- Koch, D.G., et al. 2010, *ApJ*, 713, L79
- Lucy, L. B. 1968, *ApJ* 151, 1123
- Lucy, L. B., 1976, *ApJ*, 205, 208
- McQuillan, A., Aigrain, S., & Mazeh, T. 2013, *MNRAS*, 432, 1203
- Mochnicki, S.W. 1981, *ApJ* 245, 650
- Prša, A., & Zwitter, T. 2005, *ApJ*, 628, 426
- Rappaport, S., Deck, K., Levine, A., Borkovits, T., Carter, J., El Mellah, I., Sanchis-Ojeda, R., & Kalomeni, B. 2013, *ApJ*, 768, 33
- Rappaport, S., Swift, J., Levine, A., et al. 2014, *ApJ*, 788, 114
- Rucinski, S. M. 1998, *AJ*, 116, 2998
- Slawson, R.W., Prsa, A., Welsh, W.F., et al. 2011, *AJ*, 142, 160
- Smith, J. C., Stumpe, M. C., Van Cleve, J. E., et al. 2012, *PASP*, 124, 1000

Stumpe, M. C., Smith, J. C., Van Cleve, J. E., et al. 2012, *PASP*,
 124, 985
 Tran, K., Levine, A., Rappaport, S., Borkovits, T., Csizmadia,
 Sz., & Kalomeni, B. 2013, *ApJ*, 774, 81

APPENDIX

O – *C* CURVES FOR 414 *KEPLER* BINARIES WITH ANTICORRELATED PRIMARY AND SECONDARY ETVS

We show here the *O* – *C* curves for both the primary and secondary minima of 414 short-period *Kepler* binaries. These are systems that were chosen because the primary and secondary *O* – *C* curves appear to be partially or totally anticorrelated. In all there are 23 plots each displaying the *O* – *C* curves for 18 binaries, in a 3×6 panel arrangement. The first of the 23 plots is shown here, while the remaining 22 are contained in the online-only version of the Journal.

Because the *O* – *C* curves were produced with a code different from that used by Tran et al. (2013), we provide here a brief explanation of the calculations performed to obtain *O* – *C* times for the primary minima from the detrended *Kepler* LC light curves.

Detrending of each light curve began by applying a boxcar filter with a duration of one orbital period (rounded to an integer number of long cadence time intervals). The filtered light curve was subtracted from the unfiltered curve and the overall mean of the unfiltered curve was added to the differences to form the detrended light curve. The latter is, essentially, a high-pass filtered version of the original light curve. In the following parts of this section, references to “light curve” shall be taken to mean the detrended light curve.

The basis of our timing method is the comparison of a selected interval of a folded light curve with equal duration intervals of the flux time series. The folded light curve is produced by accumulating the flux from each measurement in a histogram, where the bins of the histogram are $\tau_{LC} = 1765.46$ s in duration to match the duration of the bins in the flux time series. The bin assignment is computed from:

$$\text{bin} = \text{Int} \left\{ \frac{(t_{\text{obs}} - t_0)}{\tau_{LC}} - \text{Int} [(t_{\text{obs}} - t_0) / P_{\text{orb}}] \frac{P_{\text{orb}}}{\tau_{LC}} \right\} \quad (\text{A1})$$

where ‘Int’ is the integer function, P_{orb} is the best estimate of the orbital period (taken either from the *Kepler* binary catalog or our own determination), and t_0 is an arbitrary epoch time. The desired segment of the fold is typically of duration $30\% \times P_{\text{orb}}$ and is centered on the phase of the primary minimum. The comparison of the selected interval of the fold to an equal length interval of the flux time series is accomplished via a fit that adjusts a single scaling parameter a – defined by $lc(t) = a \times fl(\phi)$ where $lc(t)$ is the light curve and $fl(\phi)$ is the folded light curve – to yield the minimum value of χ^2 as a function of the value of a . The same segment of the folded light curve is then used to fit *every* equal length segment of the unfolded light curve. The values of χ^2 resulting from these fits form a time series with the same cadence as the flux time series. Each local minimum in the values of χ^2 considered as a time series is identified with an *O* – *C* time with an accuracy of $\pm \tau_{LC}/2$.

The *Kepler* data allow the determination of *O* – *C* times with accuracies that are much better than half of the long cadence bin time of the data. Indeed, we and others have achieved accuracies of about 10 seconds in the best cases. Some form of interpolation is necessary to achieve such accuracies, but simple interpolation algorithms are often not sufficient for obtaining times with accuracies better than ~ 100 seconds.

Our interpolation procedure is run for each coarsely determined *O* – *C* time that was determined as described above. In this interpolation procedure, the fit of the given segment of the flux time series is refit with each of a set of folded light curves. The values of t_0 of these folds are uniformly spaced over the range of $\pm \tau_{LC}/2$ with respect to the value used in the initial fit. Each fit is done over the phase interval used in the initial fit. Typically the fitting is done for 10 to 20 values of t_0 . The best value of t_0 is obtained from the fit with the minimum value of χ^2 . The supposition is that this fit corresponds to the alignment that results in the best match of the minimum value in the flux time series with the local minimum in the folded light curve; varying t_0 in this way acts like a ‘vernier scale’ on the phase measurement. Simple interpolation using the χ^2 values for the immediate neighboring values of t_0 yields the final value for this *O* – *C* time.

O – *C* times for the secondary minima were obtained in a similar fashion, except that for each *Kepler* target we searched for local minima roughly midway between primary minima. This does not work well, needless to say, for the secondary minimum of a highly eccentric orbit.

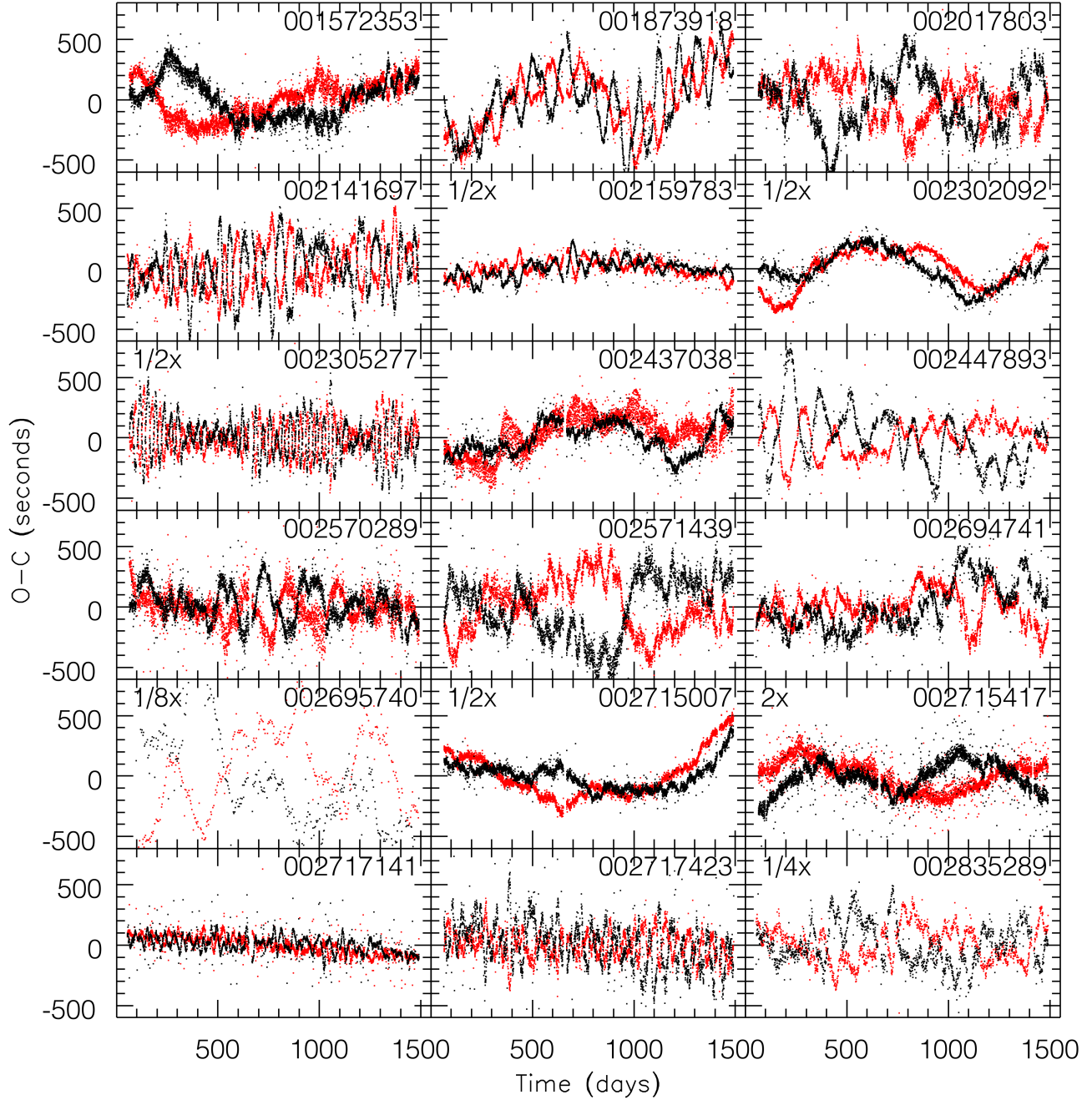


Figure 14. A set of $O - C$ curves for 18 of the 414 short-period binaries that we studied in this work. The $O - C$ curves for the primary are in black, while those for the secondary are in red. The KIC numbers are written in the upper right corner of each panel. The fraction, followed by a “x” symbol, in the upper left corner of some panels is the amount by which the $O - C$ values have been *divided* for better visibility (e.g., $1/8\times$ implies that one should multiply the displayed vertical scale by $1/8$ in order to obtain the actual $O - C$ value). Figures 15 through 36, covering all the 414 binaries in this study are available in the online-only version of the Journal.